materials

MDPI

Article

$NiTi_2$, a New Liquid Glass

Robert F. Tournier [1] and Michael I. Ojovan [2,*]

[1] UPR 3228 Centre National de la Recherche Scientifique, Laboratoire National des Champs Magnétiques Intenses, European Magnetic Field Laboratory, Institut National des Sciences Appliquées de Toulouse, Université Grenoble Alpes, F-31400 Toulouse, France; robert.tournier@lncmi.cnrs.fr
[2] Department of Materials, Imperial College London, London SW7 2AZ, UK
* Correspondence: m.ojovanl@imperial.ac.uk

Abstract: Many endothermic liquid–liquid transitions, occurring at a temperature T_{n+} above the melting temperature T_m, are related to previous exothermic transitions, occurring at a temperature T_x after glass formation below T_g, with or without attached crystallization and predicted by the nonclassical homogenous nucleation equation. A new thermodynamic phase composed of broken bonds (configurons), driven by percolation thresholds, varying from ~0.145 to $\Delta\varepsilon$, is formed at T_x, with a constant enthalpy up to T_{n+}. The liquid fraction $\Delta\varepsilon$ is a liquid glass up to T_{n+}. The solid phase contains glass and crystals. Molecular dynamics simulations are used to induce, in $NiTi_2$, a reversible first-order transition by varying the temperature between 300 and 1000 K under a pressure of 1000 GPa. Cooling to 300 K, without applied pressure, shows the liquid glass presence with $\Delta\varepsilon = 0.22335$ as memory effect and $T_{n+} = 2120$ K for $T_m = 1257$ K.

Keywords: glass; phase transitions; liquid glass; configurons; molecular dynamic simulations

1. Introduction

The classical homogenous nucleation (CHN) equation [1–4] cannot be applied above the melting temperature T_m because the melt is viewed as being homogenous, excluding the presence of intrinsic nuclei such as superclusters and superatoms, inducing crystallization after undercooling and liquid–liquid transitions above T_m [5]. The liquid–liquid transitions cannot be related to a first-order transition occurring below T_m. The undercooling of liquid elements gradually increases with overheating and reaches an undercooling plateau, which is attributed to heterogenous nucleation from oxide impurities, surface cavities, and growth kinetics dependent with the size instead of homogenous nucleation [6]. Scientists were quasi-unanimous at the end of 20th century, adopting CHN, believing that the glassy state results from liquid freezing instead of homogenous nucleation of phase transition.

The undercooling plateau is defined by the weakest reduced temperature $\theta = (T - T_m)/T_m$ where the crystallization occurs for a volume v and a nucleation time t depending on the cooling rate. The product $\theta^2 (1 + \theta)$ for $vt = 10^{-8 \pm 1}$ m^3s in the CHN equation is a linear function of $\alpha^3 S_m$ where α is proportional to the surface energy of the growth nuclei and S_m is the entropy of melting of 38 elements. In fact, this law, deduced from the CHN equation, excludes the heterogenous nucleation and promotes the homogenous nucleation and the presence of intrinsic nuclei in melts [7].

The nonclassical homogenous nucleation (NCHN) equation includes the possible presence of homogeneous nuclei, introducing in the classical equation their contribution to the Gibbs free energy [7]. The homogenous nucleation temperatures (T_{n-}) are defined by equations of two liquid states, Liquid 1 and Liquid 2 [5,8–11]. The formation of glassy phases occurs by percolation of bonds at T_g during the first cooling [12–14]. After quenching the melt below T_g, the enthalpy of formation of all bonds can relax. There are two homogeneous nucleation temperatures in Liquid 2. The highest is ($T_{n-} = T_g$); the lowest is the temperature where this enthalpy excess begins to be recovered using a slow heating rate.

check for updates

Citation: Tournier, R.F.; Ojovan, M.I. $NiTi_2$, a New Liquid Glass. *Materials* **2023**, *16*, 6681. https://doi.org/10.3390/ma16206681

Academic Editors: Lin Zhang and Zhitong Bai

Received: 11 September 2023
Revised: 25 September 2023
Accepted: 11 October 2023
Published: 13 October 2023

Copyright: © 2023 by the authors. Licensee MDPI, Basel, Switzerland. This article is an open access article distributed under the terms and conditions of the Creative Commons Attribution (CC BY) license (https://creativecommons.org/licenses/by/4.0/).

The enthalpy excesses and the recovery temperatures are found in several glasses [15–22]. The glass phase is stabilized after relaxation below the percolation threshold of broken bonds named configurons, occurring during the first heating at T_g. The specific heat undergoes a second-order phase transition at T_g with critical exponents during heating which are absent during the first cooling [23–26]. The formation of the glass phase after relaxation and broken bonds during heating is governed by the presence of a new phase, initially called Phase 3, discovered in supercooled water [27,28], having an enthalpy coefficient $\Delta\varepsilon_{lg}$ equal to the difference between those of Liquids 1 and 2 and defining the configuron enthalpy ($\Delta\varepsilon_{lg}$ H_m) [29].

The second class of homogenous nucleation reduced temperatures θ_{n+} above $\theta = 0$ respects the relation with the configuron enthalpy coefficient ($\Delta\varepsilon_{lg}$ $H_m = \theta_{n+}$ H_m) and (H_m) the melting heat of surviving entities and crystals. The configuron phase (Phase 3) undergoes a first-order transition characterized by an endothermic or exothermic latent heat equal to $|\theta_{n+} H_m|$. Consequently, the relation ($-\Delta\varepsilon_{lg} = \theta_{n+}$) is also respected because $\Delta\varepsilon_{lg}$ can be positive or negative [11]. The reduced temperature θ_{n+} above $\theta = 0$ is equal to the Scher and Zallen percolation threshold of configurons [15,30].

Exothermic transitions are induced below T_m during heating or cooling, depending on the heating and cooling rates. Undercooling with or without crystallization is observed during the first cooling depending on the cooling rate. The enthalpy coefficient $\Delta\varepsilon_{lg}$, equal to singular values of Phase 3, results from this first-order transition [31]. Heating from the glass state can produce a first-order transition between T_m and T_g with or without crystallization. The fraction $\Delta\varepsilon_{lg}$ is involved in the formation of a liquid glass up to T_{n+} and the crystallized fraction $(1 - \Delta\varepsilon_{lg})$ melts at T_m [32]. The glass fraction stabilizes nanocrystallization of any material because T_{n+} is higher than T_m. For example, volcanic rocks are composed of crystals of various sizes surrounded by glasses containing variable fractions of SiO_2.

A liquid glass is created by a first-order transition of the configuron phase to stabilize its enthalpy to a negative singular value ($-\Delta\varepsilon_{lg}$) up to T_{n+} with a specific heat equal to zero. The upper limit of $\Delta\varepsilon_{lg}$ is defined by T'_g/T_m, the glass transition temperature of the liquid glass being equal to ($T'_g = 2\,T_m - T_g$) [33,34].

Our project in this paper is to induce a first-order transition under extreme pressures in $NiTi_2$ by molecular dynamics simulations and observe the stabilization of the liquid glass, varying the temperature under constant pressure to induce a memory effect [35]. The choice of $NiTi_2$ is guided by molecular dynamics simulations showing that the glass transition occurs at (T_g = 800 K) at high cooling rate, revealing structural changes via radial distribution functions at (T_g) [36].

2. Predictions of NCHN and Configuron Models

2.1. The Nonclassical Homogeneous Nucleation (NCHN) and the Classical Homogeneous Nucleation (CHN)

In the NCHN equation, the Gibbs free energy change for a nucleus formation in a melt is given by Equation (1) [7]:

$$\Delta G_{ls} = (\theta - \varepsilon_{ls})H_m/V_m \times 4\pi R^3/3 + 4\pi R^2(1 + \varepsilon_{ls})\sigma_{ls}, \quad (1)$$

where R is the nucleus radius and following Turnbull [1], σ_{ls} is its surface energy for $\varepsilon_{ls} = 0$, given by Equation (2), θ is the reduced temperature $(T - T_m)/T_m$, H_m is the enthalpy of melting at T_m, and V_m is the molar volume:

$$\sigma_{ls}(V_m/N_A)^{-1/3} = \alpha_{ls}H_m/V_m, \quad (2)$$

The complementary enthalpy $\varepsilon_{ls} \times H_m/V_m$, introduced in the classical homogeneous nucleation (CHN) equation, authorizes the presence of growth nuclei above T_m. The prediction of an exothermic or endothermic enthalpy change, at the same temperature T_{n+} above T_m, viewed as due to the presence of antibonds or bonds, sets the NCHN

equation [33]. The CHN equation is obtained for $\varepsilon_{ls} = 0$, and leads to a homogeneous liquid above T_m in contradiction with the presence, in the liquid above T_m, of first-order transitions, and single crystal formations by cooling overheated liquid droplets.

The nucleation rate (Jvt) in a melt of volume v, after a time t, and the thermally activated energy barrier $\Delta G^*_{ls}/k_BT$ are given in Equations (3) and (4) [4]:

$$(Jvt) = (K_v vt)\exp\left(\frac{-\Delta G^*_{ls}}{k_B T}\right), \tag{3}$$

$$\frac{\Delta G^*_{ls}}{k_B T} = \frac{16\pi S_m \alpha^3_{ls}}{3N_A k_B (1+\theta)(\theta - \varepsilon_{ls})^2}, \tag{4}$$

where S_m is the entropy of melting of crystals and condensed entities [4,7]. The critical parameter $(\frac{\Delta G^*_{ls}}{k_B T})$ is not infinite at the melting temperature T_m when (ε_{ls}) is present. In this case, this event now occurs above T_m for $\theta = \varepsilon_{ls.}$ The nucleation rate is equal to 1, and Ln(Jvt) = 0 when Equation (5) is respected:

$$\Delta G^*_{ls}/k_B T = \ln(K_v vt). \tag{5}$$

The surface energy coefficient α_{ls} in Equation (2) is determined from Equations (3)–(5) and equal to Equation (6):

$$\alpha^3_{ls} = \frac{3N_A k_B (1+\theta)(\theta - \varepsilon_{ls})^2}{16\pi S_m} \ln(K_v vt). \tag{6}$$

$(S_m \alpha_{ls}{}^3)$ is effectively proportional to $(1 + \theta)\ \theta^2$ with (θ) being the reduced temperature of undercooling of 38 liquid elements, obtained after overheating the melt, using volumes v and time t with $vt = 10^{-8 \pm 1}\ m^3 s$, $K_v = 90$, Ln $(K_v vt) = 71.9 \pm 1$ in agreement with the predictions of Equation (6), as shown in Figure 1 [4].

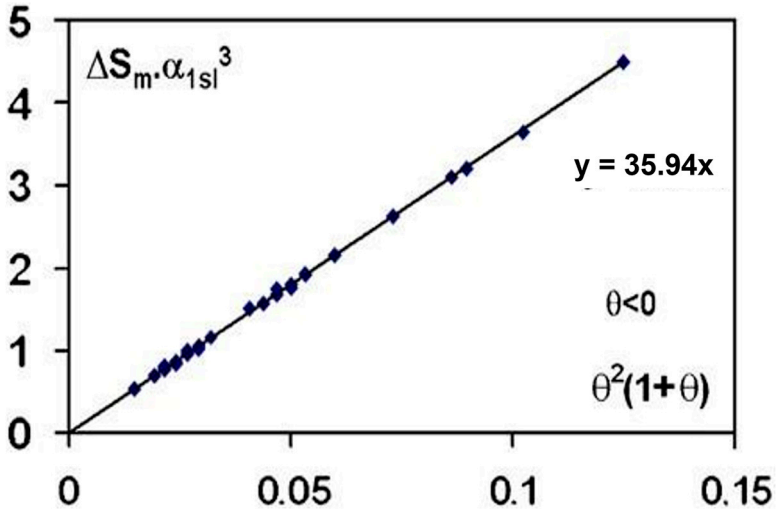


Figure 1. The quantity $\alpha^3 S_m$ is plotted as a function of $\theta^2(1 + \theta)$, θ being the algebraic lowest undercooling reduced temperature of 38 elements; α_{1ls} and S_m are, respectively, the dimensionless surface energy and the entropy of melting in JK^{-1} $mole^{-1}$. The parameters (θ) have been assembled by [4]. Reproduced from [7], Copyright 2007 Elsevier.

This law is beautifully respected in the two nucleation models and is due to homogeneous nucleation phenomena. The phase diagram of liquid elements predicts these homogenous nucleation temperatures [34]. A first-order transition occurs at the undercooling reduced temperature θ. The exothermic enthalpy is either totally attributed to crystallization with CHN without considering any homogeneous nucleation because the

liquid is viewed as being homogenous above T_m, or only partially to the nucleation of a glassy fraction depending on the nucleation temperature of first-order transition with NCHN [29,32,37]. Recent examples of these two approaches are devoted to the undercooling of $Pt_{57}Cu_{23}P_{20}$ alloy [31,38].

The nucleation temperatures θ_{n-} and θ_{n+} in the NCHN model are obtained for $d\alpha_{ls}^3/d\theta = 0$ and obey Equation (7):

$$d\alpha_{ls}^3/d\theta \sim (\theta_{n+} - \varepsilon_{ls})(3\theta_{n-} + 2 - \varepsilon_{ls}) = 0. \quad (7)$$

There are two types of homogeneous nucleation temperatures as shown by Equation (7): $\theta_{n-} = (\varepsilon_{ls} - 2)/3$ below T_m, and $\theta_{n+} = \varepsilon_{ls}$ above T_m. The first one leads to the glass formation temperature, while the second is a nucleation reduced temperature θ_{n+} above T_m obtained in many experiments, observing the undercooling versus the overheating rates of liquid elements, and glass-forming melts [39–43]. These nucleation temperatures predict, for consequence, the existence of second melting temperatures T_{n+} of growth nuclei above T_m and their growth below T_m, shown in several publications [11,32,44–57].

2.2. The Enthalpy Coefficients of Two Liquid States Depending on the Glass Transition Temperature at T_g below T_m

The NCHN model describes two liquid states characterized by enthalpy coefficients. The coefficient ε_{ls} of the initial liquid state called Liquid 1 is a quadratic function of Equation θ in Equation (8) [7]:

$$\varepsilon_{ls} = \varepsilon_{ls0}\left(1 - \theta^2/\theta_{0m}^2\right), \quad (8)$$

where θ_{0m} is the Vogel–Fulcher–Tamann (VFT) reduced temperature leading to $\varepsilon_{ls} = 0$ for $\theta = \theta_{0m}$ [8]. $(\theta^2{}_{0m})$, minimizing the complementary surface energy, is given in Equation (9) [9]:

$$\theta_{0m}^2 = \frac{8}{9}\varepsilon_{ls0} - \frac{4}{9}\varepsilon_{ls0}^2, \quad (9)$$

with $\varepsilon_{ls0} = \theta_g + 2$.

The glass transition gives rise to Liquid 2 with a new coefficient ε_{gs}, also depending on θ^2 in Equation (10) with the second VFT reduced temperature (θ_{0g}) given in Equation (11):

$$\varepsilon_{gs} = \varepsilon_{gs0}\left(1 - \theta^2/\theta_{0g}^2\right), \quad (10)$$

$$\theta_{0g}^2 = \frac{8}{9}\varepsilon_{gs0} - \frac{4}{9}\varepsilon_{gs0}^2, \quad (11)$$

with $\varepsilon_{gs0} = 1.5\theta_g + 2$, as expected with Equation (7), θ_g is the reduced glass transition temperature, and (ε_{ls0}) and (ε_{gs0}) are values for which the activation energies of Liquids 1 and 2 are equal at T_g, leading to an activation energy equal to zero for the Liquid 3 characterized by $\Delta\varepsilon_{lg} = (\varepsilon_{ls} - \varepsilon_{gs})$ [29].

2.3. Formation of New Phases through First-Order Transitions below T_m

First-order transitions are observed below T_m, depending on the heating rate. They lead to new glassy phases having a weaker enthalpy than that of the initial glass state, which is equal to zero. The enthalpy coefficient $\Delta\varepsilon_{lg}$ is equal to $-\Delta\varepsilon$ after the transition, and the first-order transition reduced temperature θ_x is determined with Equation (12):

$$\theta_x = \left(-3 \pm \left[9 - \frac{4(2 - \varepsilon_{gs0} - \Delta\varepsilon)\varepsilon_{gs0}}{\theta_{0g}^2}\right]^{0.5}\right)\frac{\theta_{0g}^2}{2\varepsilon_{gs0}} \quad (12)$$

where ε_{gs0} is the enthalpy coefficient of Liquid 2 at $\theta = 0$ given in Equation (10). This first-order reduced temperature is called θ_x, even if it is not accompanied by crystallization.

This equation is used after application of very high temperatures, and the undercooling reduced temperature is directly equal to θ_x and $\Delta\varepsilon_{lg} = -\Delta\varepsilon$ (see for example [31]).

2.4. The Glassy State of Phase 3 Up to the Melting Temperature T_{n+} above T_m

The difference $\Delta\varepsilon_{lg}$ in Equation (13) between the coefficients ε_{ls} and ε_{gs} determines the enthalpy coefficient of Phase 3 during heating and the configuron enthalpies when the quenched liquid has escaped crystallization:

$$\Delta\varepsilon_{lg}(\theta) = \left[\varepsilon_{ls} - \varepsilon_{gs}\right] = \left[\varepsilon_{ls0} - \varepsilon_{gs0} - \Delta\varepsilon - \theta^2\left(\frac{\varepsilon_{ls0}}{\theta_{0m}^2} - \frac{\varepsilon_{gs0}}{\theta_{0g}^2}\right)\right], \quad (13)$$

This phase explains the homogenous nucleation of phase transformations in supercooled water [28], and corresponds to the enthalpy coefficients of broken bonds (configurons) at the glass transition [29].

In the absence of first-order transition below T_m during the first heating, Phase 3 undergoes an exothermic transition at a reduced temperature $\theta_{n+} = \Delta\varepsilon_{lg}$, respecting Equation (7) above T_m. This transition occurs at $T_{n+} \sim 1.145\ T_m$ and corresponds to the temperature where the liquid viscosity ceases to respect the Arrhenius law during cooling from high temperature [29,58]. Rapidly quenched glass formers are amorphous and are transformed into glass phases by relaxing enthalpy during the first heating. Two liquids give rise, at first, to an intermediate Phase 3 below $T_3 < T_g$ respecting the entropy constraints, and then, the enthalpy increases towards that of the glass phase up to T_g. Phase 3 carries a medium-range order above T_g, which can be superheated above the melting temperature up to T_{n+}. The configuron model is successfully applied to 54 glasses, explaining the transitions at T_{n+} by percolation and the existence of a glassy 'ordered' fraction equal to the critical threshold of Scher and Zallen ($\Phi_c = 0.15 \pm 0.01$), producing T_g [25,30]. The temperature T_{n+} is the melting temperature of residual bonds involved in this glassy fraction [29].

First-order transitions occur in undercooled liquids at θ_x below T_m, depending on the heating rate, producing an exothermic heat equal to $-\Delta\varepsilon\ H_m$ for $\varepsilon_{gs} = 0$ in Equation (12), without crystallization [11,34,50,59–62]. The coefficient $\Delta\varepsilon$ is equal to singular values of the vitreous state enthalpy coefficient: $\Delta\varepsilon_{lg}$ (θ_{0m}), ε_{gs0}, $\varepsilon_{gs0}/2$, $\theta_{n+} \cong 0.145$, and 0. This enthalpy is recovered at various reduced temperatures $\theta_{n+} = \Delta\varepsilon$, including $\Delta\varepsilon \cong 0.145$. Two Phase 3 states with opposite enthalpies disappear at the same reduced temperature $\theta_{n+} = 0.145$ and could contain clusters-bound colloids with two opposite values of enthalpy corresponding to antibond and bond breaking. All colloid bonds disconnect at $T_{n+} > T_m$ and give rise in congruent materials, through a first-order transition at T_{n+}, forming a liquid, containing tiny superatoms, built by short-range order [33]. This description is compatible with the presence of microheterogeneities in metallic overheated liquids, as already observed by Popel et al. [45,63].

The first-order transition at θ_x induces either an enthalpy of Phase 3 being constant and equal to $-\Delta\varepsilon\ H_m$ between θ_x and θ_{n+} at high rates of cooling without crystallization, or with a crystallized (or condensed) fraction $(1 - \Delta\varepsilon)$ melted at T_m. For a fully crystallized volume, the enthalpy of crystals is assumed to be $-H_m$, considering that the denser crystalline phases lead to $\Delta\varepsilon = 1$ [64]. In the second case, the melt above T_m contains a glassy fraction $\Delta\varepsilon$ and a homogeneous liquid fraction equal to $(1 - \Delta\varepsilon)$. This mixed state leads to the formation of crystals, coexisting with a glass fraction up to T_m with a glass state stable up to T_{n+} [11,26,31–33].

2.5. The Formation of a Liquid Glass above T_m

The formation of a liquid glass is expected at a temperature ($T'_g = 2\ T_m - T_g$) [32]. A glass transition at θ_g is accompanied at high temperatures by a second glass transition occurring at $-\theta_g$ above T_m. This phenomenon is a consequence of the θ^2 dependence of the enthalpy of glass phases. The corresponding VFT temperature squares are negative at high temperatures and the values of ε_{gs0} and ε_{ls0} become higher than 2. These glass

transitions have been already observed three times without being recognized as liquid glasses by the experimentalists [65–68]. The two transitions occur at T_g = 715 K and T'_g = 1535 K in $Cu_{46}Zr_{46}Al_8$ with T_m = 1125 K, during cooling of the melt, accompanied by an exothermic transition [32,65]. In the second material, the composite (ZIF-62) (Al-rich) (50/50) has a solidus melting temperature at 650 K, T_g = 591 K and T'_g = 709 K observed during heating and accompanied by an endothermic latent heat. A glass transition still exists in tin far above T_m, and looks like a partial glassy fraction by [34,68]. A liquid glass is observed in suspensions of ellipsoidal colloids [69].

2.6. Validation of NCHN with Molecular Dynamics Simulations

A phase diagram of ice in single-walled carbon nanotubes at atmospheric pressure is established by numerical simulations, and predicts ice melting points as a function of their diameter up to 1.7 nm [70]. All of these melting points agree with the temperatures T_{n+} given by the NCHN equation [37]. A first-order transition from liquid to homogenous glass, denoted L-glass, is predicted with the NCHN equation since 2016, in liquid elements, having a Lindemann constant close to 0.103, accompanied by a latent heat of 10.5% of the melting heat [10]. The transition under pressure of ^{4}He is the first example of this phenomenon [71]. Recent molecular dynamics simulations identify, in addition, a first-order transition at T_x from liquid (L) to a metastable heterogenous solid-like phase, denoted as G-glass, when a supercooled liquid evolves isothermally below its melting temperature T_m at deep undercooling [59,61]. The NCHN model describes the first-order transitions from liquid to L-glass and to G-glass in agreement with these simulations [62,72]. The G-glass is a heterogenous phase consisting of regions fully embedded in a surrounding disordered medium.

Molecular dynamics simulations show full melting at T_{n+} = 1.119 T_m for Zr [60], 1.126 T_m for Ag [61], 1.219 T_m for Fe, and 1.354 T_m for Cu [73]. The NCHN model applied to liquid elements is based on the increase of the Lindemann coefficient with the heating rate. The glass transition at T_g and the nucleation temperatures of G-phases at T_x and their melting at T_{n+} are predicted. A universal law relating T_{n+} and T_x shows that T_x cannot be higher than 1.293 T_m for T_{n+} = 1.47 T_m. The enthalpies of G-phases have singular values, corresponding to the increase of percolation thresholds with T_g and T_x above the Scher and Zallen invariant at various heating and cooling rates [62].

As a conclusion of this chapter, the liquid glass states extend far above T_m. Varying pressures and temperatures and formation conditions of liquid glasses could be determined. For that purpose, a study of glass states and liquid glass states of ($NiTi_2$) [36,74] under pressure by molecular dynamics simulations is developed in the next chapter.

3. Numerical Simulations

Molecular dynamics (MD) computer simulation using a open source code – software package for classical molecular dynamics Large-scale Atomic/Molecular Massively Parallel Simulator (LAMMPS, https://www.lammps.org/#gsc.tab=0 accessed on 29 October 2020) at periodic boundary conditions was used for modeling [75]. The simulation was performed at a 1 fs time step using the embedded atom potential derived for Ti–Ni alloys [76]. An atomic cell containing 128,000 atoms was heated to 2500 K to melt, and then cooled down to produce a glass. Melting was confirmed by the radial distribution function and stabilization of the density variation with time. A thermostat was used to control the temperature [77,78], while pressure was maintained by a barostat [79].

Deviations and irreproducibility have been studied using these types of coupling to determine possible deviations in dynamic properties for time constants as low as 0.01 ps. Reliable and thermostable dynamic properties can be derived for coupling time constants above 0.1 ps [80]. The atomic volume is calculated here using coupling time constants much higher than 10^{-13} s. The weakest time (10^{-13} s) would correspond to a temperature variation of 1 K without a change of dV_{at}/dT. The highest time used in these simulations is 3×10^{-10} s. The atomic volume variation under a pressure of 1000 GPa is

$dV_{at}/dp = 1.7881 \times 10^{-7}$ with p in bars at a constant temperature of 299.7 K. The typical pressure variation is ~10,000 bars, leading to $\Delta V_{at} = 1.788 \times 10^{-3}$ Å^3. Changing the temperature of 1 K has no influence on dV_{at}/dp. Typical variations (ΔT) at ambient pressure are ~5 K. The reproducibility of the simulation during several cycles of temperature and pressure shows that the limit of ~10^{-13} s has no influence on the results because the times of coupling are much higher than 0.1 ps.

4. $NiTi_2$, a New Liquid Glass

4.1. The Vitreous States of $NiTi_2$ with T_g = 800 K and 695.5 K

The glass transition of $NiTi_2$ is equal to 800 K with a cooling rate of $10^{12}-10^{13}$ K/s and ~700 K [36] for an experimental value obtained on heating [74]. $NiTi_2$ is chosen because its glass transition, at T_g = 800 K, and at high cooling rate, was initially determined by molecular dynamics simulations [36].

The enthalpy coefficients calculated with Equations (7)–(13), representing the enthalpy coefficient of Phase 3 in Figure 2, are given below in Equation (14), and are those of a fragile glass with T_m = 1257 K [80] and T_g = 800 K:

$$\begin{gathered}\theta_g = (800-1257)/1257 = -0.36356;\ \varepsilon_{lso} = \theta_g + 2 = 1.63644;\ \varepsilon gs_0 = 1.5\theta_g + 2 = \\ 1.45466,\ \theta^2_{0m} = \tfrac{8}{9}\varepsilon_{lso} - \tfrac{4}{9}\varepsilon^2_{lso} = 0.264422;\ \theta^2_{0g} = \tfrac{8}{9}\varepsilon_{gs0} - \tfrac{4}{9}\varepsilon^2_{gs0} = 0.352573; \\ \text{Liquid 1}:\ \varepsilon_{ls} = 1.63644\left(1-\theta^2/0.264422\right);\ \text{Liquid 2}:\ \varepsilon_{gs} = 1.45465 \\ (1-\theta^2/0.352573);\ \text{Phase 3}:\ \Delta\varepsilon_{lg} = \varepsilon_{ls} - \varepsilon_{gs} = 0.18178 - 2.0629 \times \theta^2\end{gathered} \tag{14}$$

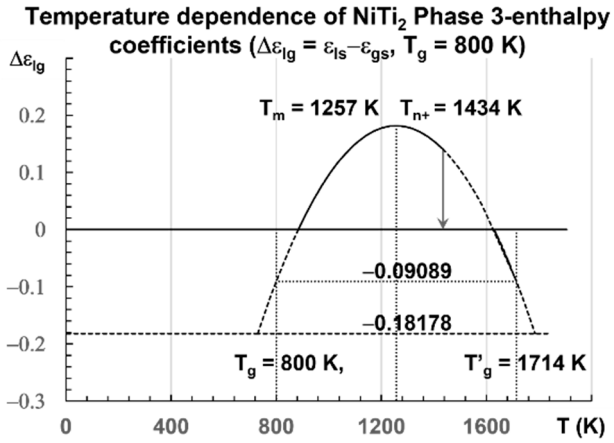


Figure 2. Temperature dependence of $NiTi_2$ configuron enthalpy for T_g = 800 K. The enthalpy coefficient ($\Delta\varepsilon_{lg}$) of Phase 3 given in Equation (13) is plotted as a function of the temperature in Kelvin for a fragile liquid with T_g = 800 K. The singular values $(\Delta\varepsilon_{lg}) = -\Delta\varepsilon_{gs0} = -0.18178$ of Phase 3 and zero in the glass state are observed. The two others $\Delta\varepsilon_{gs0}/2 = 0.09089$ and $\Delta\varepsilon_{lg}(\theta_{0m}) = 0.36369$ are not obtained at room temperature. An exothermic first-order transition is expected at T_{n+} = 1434 K with $\theta_{n+} = \Delta\varepsilon_{lg} = 0.14085$ at a low heating rate.

The singular values of $\Delta\varepsilon_{lg}$ are calculated with Equation (14) for various values of θ: $\Delta\varepsilon_{gso} = 0.18178$ (θ = 0), $\Delta\varepsilon_{gso}/2 = 0.09089$ (θ = θ_g), $\Delta\varepsilon_{lg}(\theta_{0m}) = 0.36369$ $\theta^2_{0m} = 0.264422$), $\Delta\varepsilon_{lg} = 0.14085$ for θ = 0.14085, and $\Delta\varepsilon_{lg} = 0$ (θ = −0.29685). They are the enthalpy coefficients of the configuron phase which are determined during the first heating after the first cooling from a temperature higher than T_m.

The liquid glass transition would be $T'_g = 2T_m - T_g = 1714\text{K}\left(\theta'_g = +0.36356\right)$ at the end of the first heating after the formation of broken bonds (configurons).

The enthalpy coefficient ($\Delta\varepsilon_{lg}$) of Phase 3 is −0.18178 for T_g = 800 K [36] with cooling rates of $10^{12}-10^{13}$ K/s and −0.22335 for T_g = 695.5 K at a low heating rate [74]. A transition is expected at T_{n+} = 1434 K for a liquid with T_g = 800 K, being quenched from temperatures near T_m and heated at 0.3 K/s [32]. Many exothermic or endothermic transitions have

already been observed at these temperatures [42,44–46,48,52–54]. Recent study confirms the existence of these temperatures $T_{n+} > T_m$ in all liquids previously vitrified at low temperatures [29]. All these transitions correspond to the temperature below which the Arrhenius law is no longer working, occurring at $T_{n+} \cong 1.145\ T_m$ [58]. They are glass transitions of the fraction (≅0.1445) of unbroken bonds, equal to the percolation threshold predicted by the configuron model and the Scherr and Zallen invariant [25,26].

The enthalpy coefficients for $T_g = 695.5$ K and $T_m = 1257$ K, used in Figure 3, are given below in Equation (15) [8,32,74]:

$$\begin{gathered}\theta_g\ (695.5-1257)/1257=-0.446698;\ \varepsilon_{lso}=\theta_g+2=1.55330;\ \varepsilon gs_0=1.5\,\theta_g+2=\\ 1.32995,\ \theta_{0m}^2=\tfrac{8}{9}\varepsilon_{lso}-\tfrac{4}{9}\varepsilon_{lso}^2=0.388381;\ \theta_{0g}^2=\tfrac{8}{9}\varepsilon_{gs0}-\tfrac{4}{9}\varepsilon_{gs0}^2=0.396058\ [8],\\ \text{Liquid 1: } \varepsilon ls = 1.55330(1-\theta^2/0.388381),\ \text{Liquid 2: } \varepsilon_{gs} = 1.553302(1-\\ \theta^2/0.396058),\ \text{Phase 3: } \Delta\varepsilon_{lg}(\theta)=\varepsilon_{ls}-\varepsilon_{gs}=0.22335-1.679\times\theta^2;\ T_g=695.5\ \text{K}\\ [74]\ \text{and}\ \theta_g=-0.446698\ \text{and}\ T'_g=2\,T_m-T_g=1818.5\ \text{K}\ \text{and}\ \theta'_g=0.446698\ [32].\end{gathered} \tag{15}$$

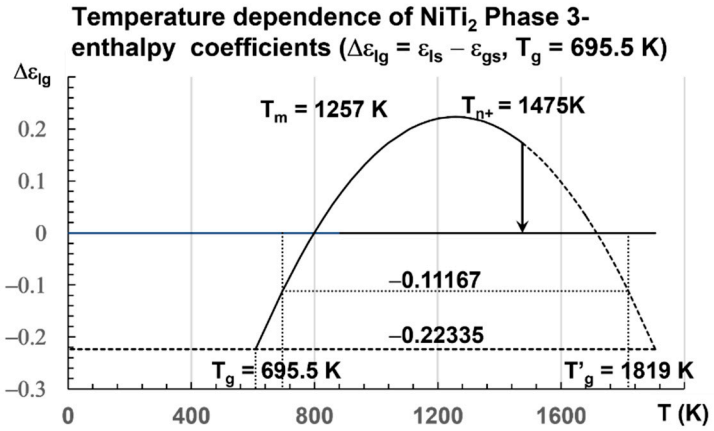


Figure 3. Temperature dependence of $NiTi_2$ configuron enthalpy for $T_g = 695.5$ K. The enthalpy coefficient ($\Delta\varepsilon_{lg}$) of Phase 3 given in Equation (15) is plotted as a function of the temperature in Kelvin for a fragile liquid with $T_g = 695.5$ K. The singular values ($\Delta\varepsilon_{lg}$) = $-\Delta\varepsilon_{gs0} = -0.22335$ of Phase 3 and zero of the glass state are observed. The two others $\Delta\varepsilon_{gs0}/2 = 0.11167$ and $\Delta\varepsilon_{lg}(\theta_{0m}) = 0.29442$ are not obtained at room temperature. An exothermic first-order transition is expected at $T_{n+} = 1475$ K with $\theta_{n+} = \Delta\varepsilon_{lg} = 0.17306$ at a low heating rate.

A transition is expected at slow heating at $T_{n+} = 1475$ K for a liquid being quenched from temperatures much closer to T_m. The enthalpy coefficient of Phase 3 is −0.22335. The volume change calculated by numerical simulations is equal to $0.22335 \times 1.5661 = 0.3498 \pm 2\%$. The coefficient $1.5661 \pm 1\%$ transforms the enthalpy coefficient −0.22335 in a volume change in $Å^3$ at the melting temperature T_m because the enthalpy of melting is equal to the enthalpy variation between T_m and $2\ T_m$ [34]. Simulations of the volume are used to predict this coefficient of $1.5661 \pm 1\%$. The transition at T_{n+} is expected at 1475 K, a temperature where $\theta_{n+} = \Delta\varepsilon_{lg} = 0.17306$.

4.2. The Atomic Volume Hysteresis above the Melting Temperature Up to 2120 K

The $NiTi_2$ atomic volume V_{at} in Angström^3, represented by the red line in Figure 4, is obtained by cooling the melt from 3000 K to 300 K, and is equal to 15.2829 $Å^3$ at 300 K.

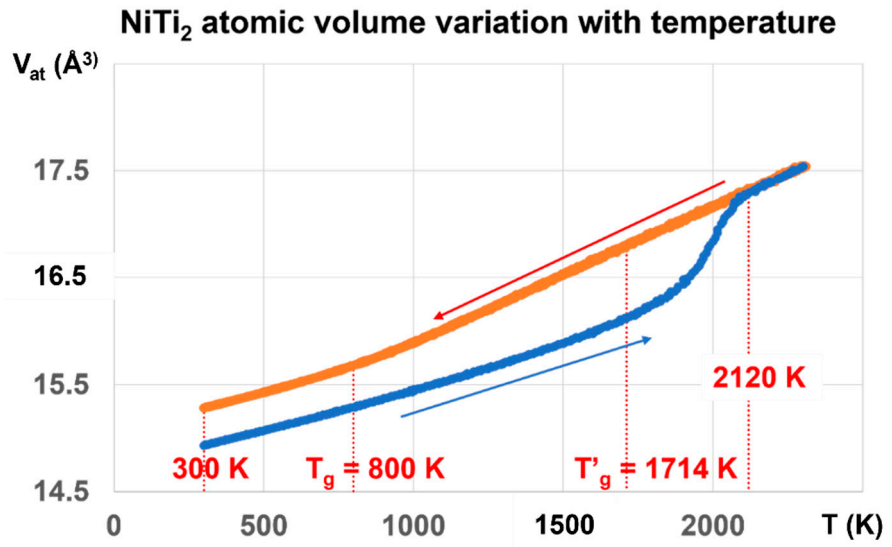


Figure 4. $NiTi_2$ atomic volume variation with temperature using cooling and heating rates of 10^{13} K/s. Two values of the atomic volume are observed and fixed by the thermal history under pressure. The red line is obtained by decreasing the temperature from 3000 K down to 300 K under pressures weaker than 700 bars. The first glass transition occurs at 800 K during cooling. The melt is submitted to a glass transition at 2120 K during heating. The atomic volume along the blue line is very stable from 300 to 800 K, whatever the pressure of ±700 bars is, and results from a first-order transition, under a pressure of 1000 GPa at 1000 K, varying the temperature to 300 K, and finally decreasing the pressure to 1 bar. The glass phase totally disappears at 2120 K instead of 1714 K.

The atomic volume represented by the blue line starts at 300 K from V_{at} = 14.9331 Å^3 obtained after applying a pressure of 1000 GPa at 1000 K, lowering the temperature down to 300 K, and finally decreasing the pressure to 1 bar. The hysteresis cycle between 300 and 3000 K is measured under weak pressures P, varying between −660 bar and +700 bar. The line thicknesses include the volume variations with pressure. The atomic volume follows the blue line during reheating up to 2120 K. Above this temperature, the blue and red lines merge, and the volume is reproducible with pressure increase or decrease. The glass transition temperature occurs at 2120 K without volume jump.

The temperature T'_g = 1714 K is equal to (2 T_m − T_g) with T_m = 1257 K and T_g = 800 K. The temperature of 2120 K corresponds to θ_{n+} = 0.68632, being equal to the sum of singular enthalpy coefficients (0.14085 + 0.18178 + 0.36369) of Phase 3 with T_g = 800 K, and determining the highest glass transition temperature of Phase 3 and the highest melting temperature of $NiTi_2$, as already observed for several liquid elements [62].

The first-order transition of the glass phase expected at T'_g = 1714 K is not observed by heating from low temperatures. Nevertheless, ΔV_{at}, the difference between the red and blue lines, is maximum at this temperature and decreases to zero from 1714 K to 2120 K. In addition, it is constant from 300 K up to the first glass transition at T_g = 800 K where ΔV_{at} begins to increase with the temperature.

The glass transition at 800 K is observed on the red curve by the slope change of V_{at} at this temperature while a new glass state is induced by a first-order transition, occurring at 1000 GPa by decreasing the temperature from 1000 to 300 K, followed by lowering the pressure down to 1 bar. This new glass state disappears during heating at 2120 K. The $NiTi_2$ melt cooled from 3000 K to 800 K does not undergo liquid glass transformation.

4.3. The First-Order Transition under 1000 GPa

A liquid glass state is revealed in Figure 5 by a first-order transition as expected. An atomic volume change, equal to −0.00979 Å^3 under 1000 GPa, is induced by a reduction of temperature from 1000 K to 300 K and by the memory of this transition, as shown in Figure 4.

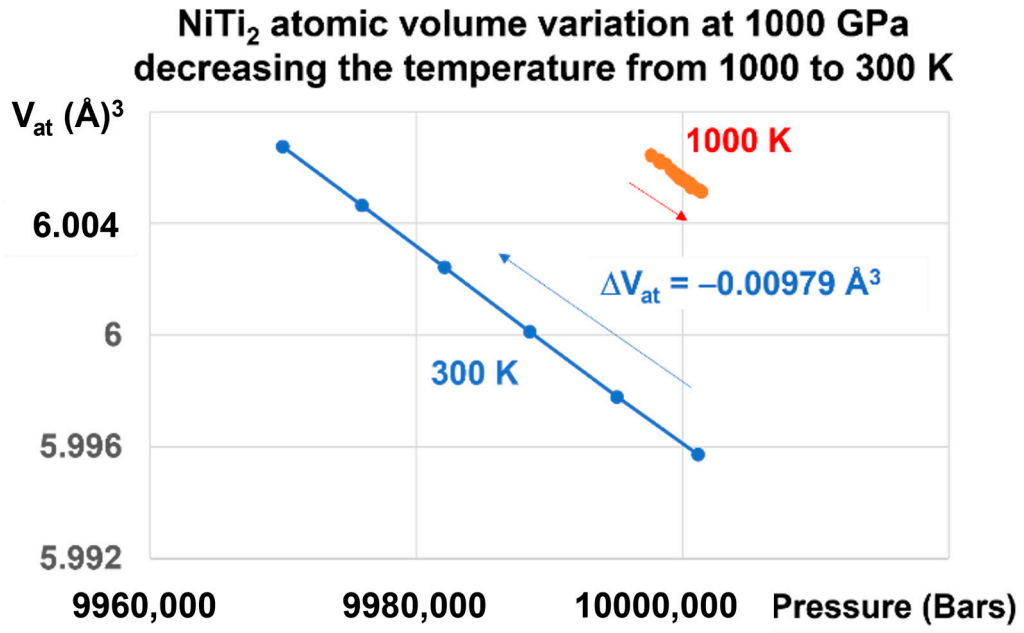


Figure 5. $NiTi_2$ atomic volume variation at 1000 GPa, decreasing the temperature from 1000 to 300 K. Increasing the pressure at T = 1000 K up to 1000 GPa and lowering the temperature down to 300 K induces a first-order transition in the glass state accompanied by a volume change equal to $\Delta V = -0.00979$ Å^3.

A memory effect has been numerically predicted in a three-dimensional model for structural glass when submitted to a temperature cycle [35]. Here, a first-order transition is observed and builds a memory effect.

This transition is reversible, as shown in Figure 6.

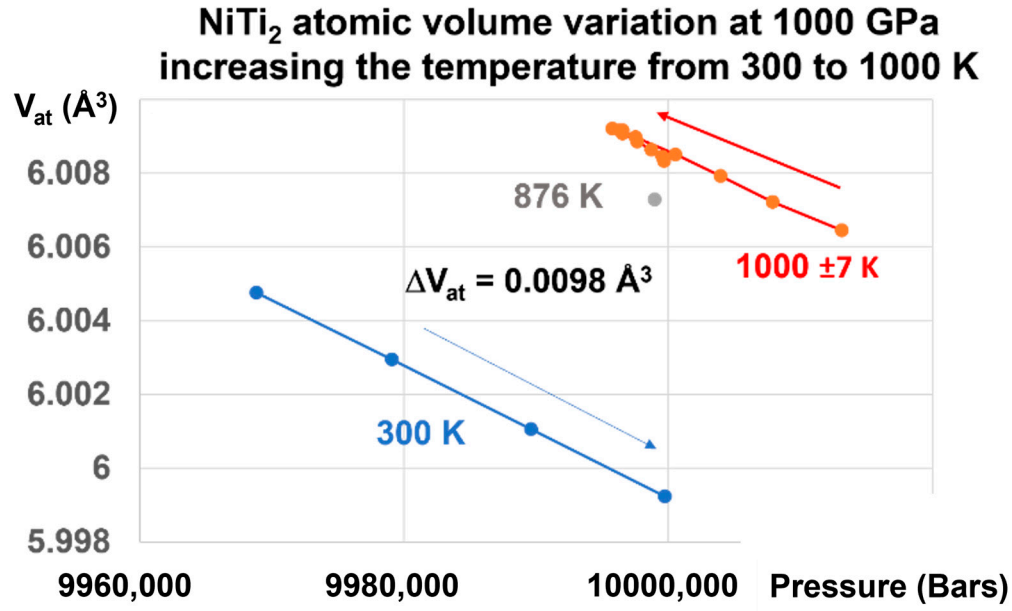


Figure 6. $NiTi_2$ atomic volume variation at 1000 GPa, increasing the temperature from 300 to 1000 K. Increasing the pressure on the glass state at T = 300 K up to 1000 GPa and increasing the temperature from 300 K to 1000 K induces a first-order transition from the glass to the liquid state, and a volume change of +0.00980 Å^3, equal to that observed in Figure 5.

Applying a pressure of 1000 GPa at 300 K and increasing the temperature to 1000 K induces an increase of the atomic volume of 0.0098 Å^3, as shown in Figure 6. This transfor-

mation reduces the difference (ΔV_{at}) = −0.3498 Å^3 at 300 K, as shown in Figure 4, to a value which is 35.69 times weaker. This factor (35.69) is related to the increase of the melting heat under pressure.

4.4. The Phase Diagram of Glass Phases in Fragile Liquids

The phase diagram in Figure 7 is devoted to Phase 3 of fragile liquids, having a melting temperature (T_m) and submitted to first-order transitions induced at T_x/T_m and T_g/T_m at various heating rates from their low temperature glass state. The ratio of T_g/T_m of fragile glasses is always higher than 0.5 ($\theta_g > -0.5$). This limit corresponds to Vogel–Fulcher–Tamann temperatures higher than $T_m/3$. The reduced glass transition at θ_g is varying from −0.5 to 2.581 and T_g/T_m from 0.5 to 3.581. For each value of θ_g, there are first-order transitions of Phase 3, occurring at θ_x and θ_{n+}, accompanied by enthalpy coefficient changes respectively equal to $-\Delta\varepsilon$ and $+\Delta\varepsilon$. For example, $T_x/T_m = 0.22335 = \Delta\varepsilon$ leads to two glass transitions at $T'_g/T_m = 0.5487$ and 3 ($\theta_g = -0.77665$ and 2) at zero pressure and constant melting temperature.

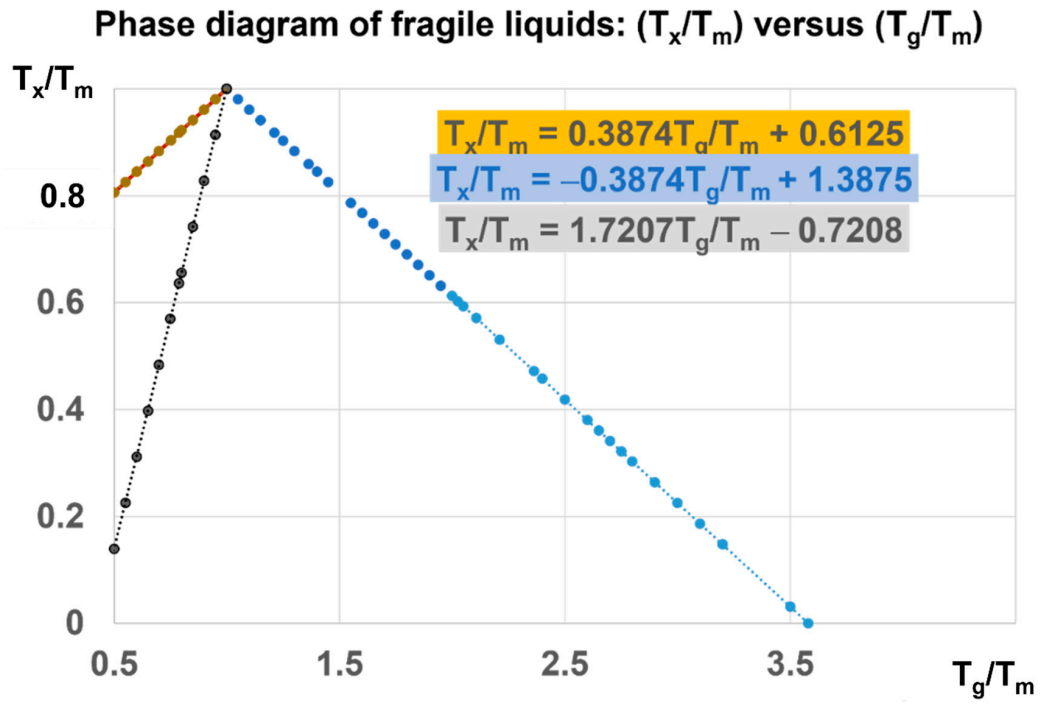


Figure 7. Phase diagram of fragile liquids: (T_x/T_m) versus (T_g/T_m). For each value of T_x/T_m, higher than 0.8 at zero pressure, there are two glass transitions corresponding to T_g and T'_g. For $T_x/T_m > 0.13962$, there is a unique glass transition $T'_g/T_m < 3.22076$. A pressure has, for consequence, to reduce T_x/T_m and to increase T_g/T_m beyond 3.22076. This ratio tends to the upper limit equal to 3.581 when the pressure tends to infinite.

There are two types of first-order transitions at T_x. In the first case, the Phase 3 enthalpy falls to $-H_m$ at T_x, remains constant up to T_m, and an enthalpy fraction $\Delta\varepsilon$ is recovered through a new first-order transition at T_{n+} far above T_m. Consequently, the melting enthalpy, recovered at T_m, is reduced and equal to $(1 - \Delta\varepsilon)\ H_m$. The temperature ($T_{n+}$), corresponding to a reduced temperature equal to $\theta_{n+} = \Delta\varepsilon$, is the glass transition reduced temperature of the liquid fraction $\Delta\varepsilon$, which is not crystallized or condensed at T_x [31,34]. This diagram is also used to predict the glass transitions under pressure, taking account of the pressure dependence of T_m and H_m.

In the second case, the transition at T_x is not accompanied by a crystallized or a condensed fraction, and is only due to the formation of various Phases 3, having enthalpies equal to $-\Delta\varepsilon\ H_m$ with $\Delta\varepsilon$ also equal to singular values of percolation thresholds of config-

urons in Equation (14): $\Delta\varepsilon_{sg0}$ ($\theta = 0$), $\Delta\varepsilon_{sg0}/2$ ($\theta = \theta_g$), $\Delta\varepsilon_{lg}$ ($\theta = \theta_{0m}$), $\Delta\varepsilon_{lg}$ (θ_{n+}), and zero. There is no crystalline phase. The volume difference ΔV_{at} increases with temperature up to $T'_g = 1714$ K. The liquid fraction [$\Delta\varepsilon = (T'_g - T_m)/T_m$] participates to the glass state up to T'_g.

The enthalpy changes, associated with the first-order transitions at $T_{n+} = T_g$ and T_x, are, respectively, equal to $\pm\Delta\varepsilon\ H_m$. The melting heat H_m increases with pressure, while ($\Delta\varepsilon$) decreases as $1/H_m$. The value of $\Delta\varepsilon$ is divided by 35.69 under a pressure of 1000 GPa because the melting heat is multiplied by 35.69. Consequently, ($\Delta\varepsilon$) = 0.0098 at 1000 GPa leads to $T_g/T_m = (3.581 - 0.0098/0.581) = 3.5641$ near the upper limit of 3.581, as shown in Figure 7.

4.5. The Melting Temperature Increases with Pressure

The melting entropy is 9.3 J/K/mole in many metals, and the melting heat is quasi-proportional to T_m [4]. The pressure application increases the liquid entropy proportionally to the induced melting temperature. Consequently, the melting heat is expected to be proportional to $T_m{}^2$ and a linear function of the pressure (P), as shown for $NiTi_2$ in the following equations:

assuming $\Delta\varepsilon = 0.22335$ for $T_g = 695.5$ K

$$\left(\frac{T_m}{T_0}\right)^2 = 1 + 34.69/1000 \times P(GPa) \quad (16)$$

and assuming $\Delta\varepsilon = 0.18178$ for $T_g = 800$ K

$$\left(\frac{T_m}{T_0}\right)^2 = 1 + 28.08/1000 \times P(GPa) \quad (17)$$

where T_0 is the melting temperature at ambient pressure and P is the pressure in GPa. The equation for $T_g = 695.5$ K works and results from the decrease of T_g from 800 K to 695.5 K at ambient temperature and pressure. The glass transition temperature at the pressure of 1000 GPa is $T_g = 800$ K. Then, the most probable melting temperature is $T_m = 6779$ K at this pressure, given by Equation (17) for $T_g = 800$ K.

At P = 0, T_m is equal to $T_0 = 1257$ K [80]. For P =1000 GPa, $(T_m/T_0)^2 = 35.69$ or 29.08, in agreement with the numerical simulations. (T_m) under P = 1000 GPa is 7509 K or 6779 K. The dependence of T_m with P is given in Table 1, using the two values (0.22335) and (0.18178) of $\Delta\varepsilon$. For P = 500 GPa, $\Delta\varepsilon$ and ΔV_{at} are multiplied by 1.948 compared to ΔV_{at} at 1000 GPa. The volume change, calculated at 1000 GPa, is 2% or 3.6% weaker than the simulated value (0.00979). The glass transition even increases at pressures much higher than 1000 GPa, with ΔV_{at} tending to zero.

This linear law of variation with $T_m{}^2$ with pressure has never been used. It is then important to apply it to other known metals. Copper and iron are chosen. There are many measurements of copper at low pressures [81–85]. The initial slope varies between 36.4 and 47.7 K/GPa. These measurements lead to the two following laws, Equations (18) and (19) for copper, in good agreement with many experimental and theoretical results:

$$\left(\frac{T_m}{T_0}\right)^2 = 1 + 34.69/1000 \times P(GPa), \quad (18)$$

$$\left(\frac{T_m}{T_0}\right)^2 = 1 + 47.7/1000 \times P(GPa), \quad (19)$$

which are represented in Figure 8, together with those of $NiTi_2$ and Fe. For Cu, our extrapolated values in 500 GPa are 7253 K and 8299 K, in agreement with $T_m = 7900$ K [82]. From another determination in 100 GPa, $T_m = 3900$ K [86], and our values are 3463 K and 3905 K.

Table 1. Four first columns on the left are devoted to the liquid having T_g = 695.5 K, while the four last columns on the right to T_g = 800 K. Values of T_m, $\Delta\varepsilon$, and ΔV_{at} are given as a function of pressure in GPa respecting Equations (16) and (17).

P (GPa)	T_m	$\Delta\varepsilon$	ΔV_{at} (Å^3)	P (GPa)	T_m	$\Delta\varepsilon$	ΔV_{at}(Å^3)
0	1257.0	0.22335	0.34979	0	1257.0	0.18178	0.28469
30	1795.7	0.10945	0.17141	30	1706.2	0.09866	0.15452
60	2206.5	0.07248	0.11352	60	2059.6	0.06771	0.10604
100	2657.3	0.04998	0.07827	100	2452.9	0.04774	0.07476
150	3130.8	0.03600	0.05639	150	2869.7	0.03488	0.05462
250	3909.4	0.02309	0.03616	250	3559.8	0.02267	0.03550
350	4556.8	0.01700	0.02662	350	4136.3	0.01679	0.02629
450	5123.0	0.01345	0.02106	450	4641.7	0.01333	0.02088
500	5383.9	0.01217	0.01907	500	4874.8	0.01209	0.01893
600	5870.9	0.01024	0.01604	600	5310.4	0.01018	0.01595
700	6320.5	0.00883	0.01383	700	5712.9	0.00880	0.01378
800	6740.1	0.00777	0.01217	800	6088.9	0.00775	0.01213
900	7135.2	0.00693	0.01086	900	6442.9	0.00692	0.01084
1000	7509.5	0.00626	0.00980	1000	6778.5	0.00625	0.00979

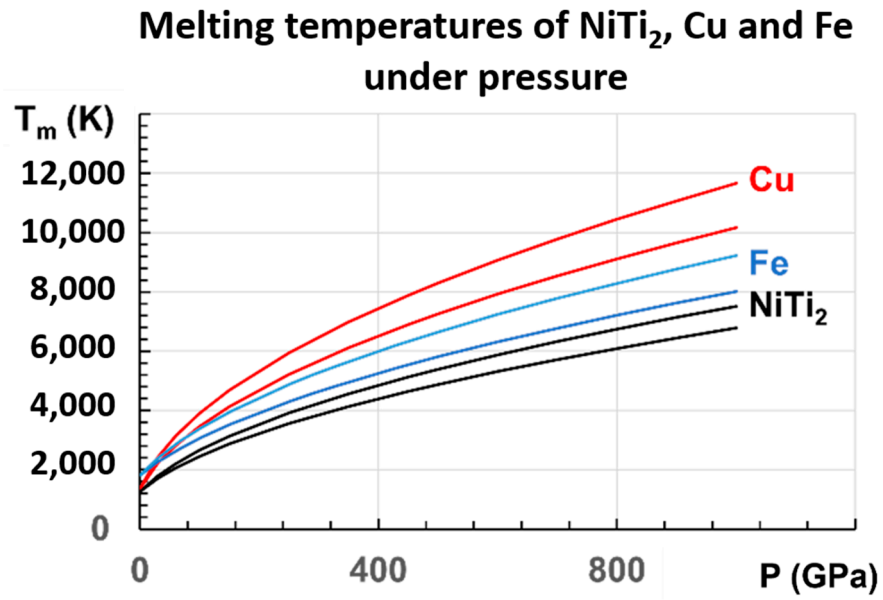


Figure 8. The melting temperatures of Cu, Fe, and $NiTi_2$ are represented versus P (GPa), following the proposed equations: for Cu: (18,19); for Fe: (20,21); for $NiTi_2$: (16,17).

For Fe, recent measurements up to 103 GPa are determined by X-ray absorption spectroscopy up to 103 GPa, and used to predict a melting temperature of 4850 ± 200 K at the inner core boundary (ICB) of the earth for P = 330 GPa [87]. Another melting temperature of 5500 ± 220 K at the ICB has been extrapolated from a measurement under P = 290 GPa in a resistance-heated diamond-anvil cell [88].

An extrapolation of this experimental result yields a melting point of 5500 ± 220 K at the ICB, higher than the previous reported result. Two laws, Equations (20) and (21) for iron, are deduced from our model, respectively, based on the works of Aquilanti et al. [87] and Sinmyo et al. [88].

$$\left(\frac{T_m}{T_0}\right)^2 = 1 + 18.56/1000 \times P(GPa), \quad (20)$$

$$\left(\frac{T_m}{T_0}\right)^2 = 1 + 24.92/1000 \times P(GPa), \quad (21)$$

Our extrapolation, at 330 GPa from measurements below 103 GPa, leads to T_m = 4834 K, in agreement with the evaluation of 4850 ± 200 K [88].

4.6. Increase of the Enthalpy Difference between Liquid and Glass with Temperature from 300 K to 1734 K

The difference ΔV_{at} is equal to 0.3498 Å^3 under pressure variations between ±700 Bars from 300 K to 700–800 K, as shown in Figures 4 and 9.

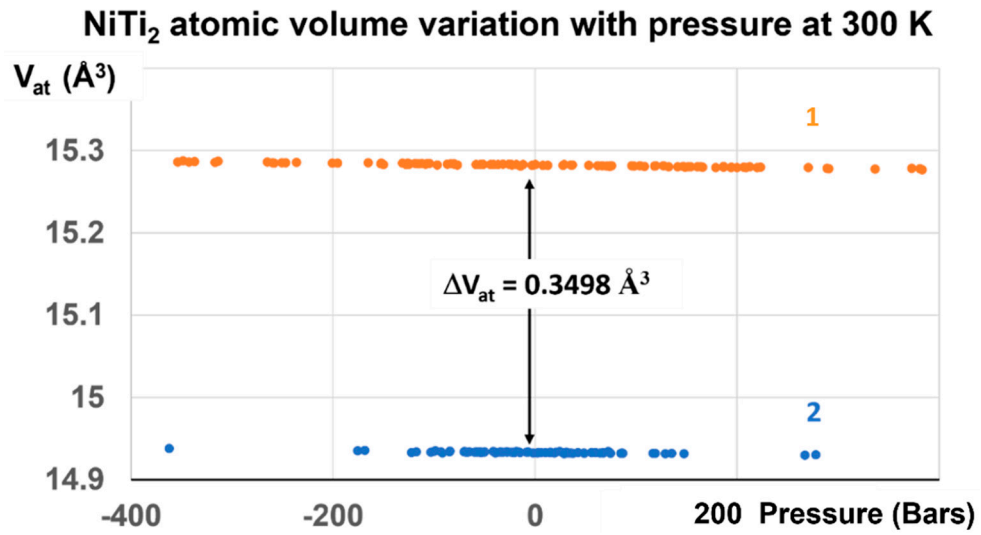


Figure 9. $NiTi_2$ atomic volume variation with pressure at 300 K. Two stable volumes at room temperature and under atmospheric pressure are obtained after the first-order transition induced at 1000 GPa. The volume difference ΔV_{at} at 300 K between liquid, noted 1, and glass, noted 2, is equal to 0.3498 ± 0.004 Å^3, and corresponds to that of configurons for T_g = 695.5 K.

The glass state, induced by the first-order transition, exists up to T'_g =1714 K for T_g = 800 K with ΔV_{at}, increasing from 0.3498 to 0.6808 Å^3, as shown in Figure 10.

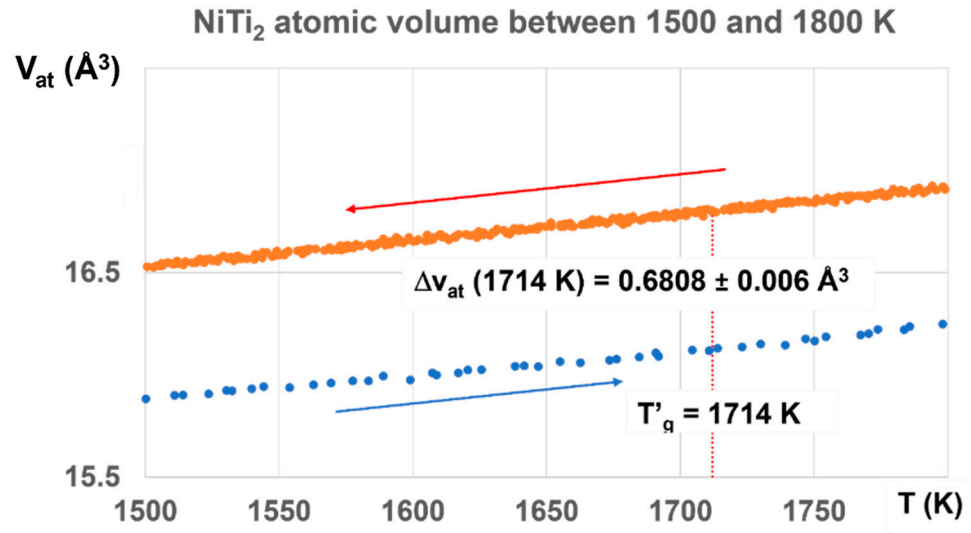


Figure 10. $NiTi_2$ atomic volumes between 1500 and 1800 K. The atomic volume difference increases with temperature up to ΔV_{at} = 0.6808, corresponding to $\Delta\varepsilon$ = 0.6808/1.5661 = 0.4387, a value a little weaker than T'_g/T_m = 1818.5/1257 = 0.4467, and much higher than T'_g/T_m = 1714/1257 = 0.36356 (q'_g = 0.36356). The melt has a glass transition temperature much closer at T'_g = 1818.5 K (T_g = 695.5 K) than T'_g = 1714 K (T_g = 800 K).

The value of ΔV_{at} at T'_g = 1714 K would correspond to a first-order transition under 1000 GPa induced by a temperature increase from 300 to 1724 K with ΔV_{at} = 0.6808/36.73 = 0.0185 ± 0.0016. This continuous increase of ΔV_{at} up to T'_g indicates that a high fraction volume of the sample belongs to a glass phase.

The enthalpy coefficient of Phase 3 with ΔV_{at} = 0.6808 corresponds in fact to $\Delta\varepsilon$ = 0.6808/1.5661 = 0.4387, a value a little weaker than θ'_g = (1818.5 − 1257)/1257 = 0.4467, and much higher than θ'_g = (1714 − 1257)/1257 = 0.36356. The melt has a glass transition temperature much closer at T'_g = 1818.5 K (T_g = 695.5 K) than T'_g = 1714 K (T_g = 800 K). The coefficient $\Delta\varepsilon$ tends to decrease toward 0.36356, corresponding to T'_g = 1714 K and T_g = 800 K, as shown in Figure 11.

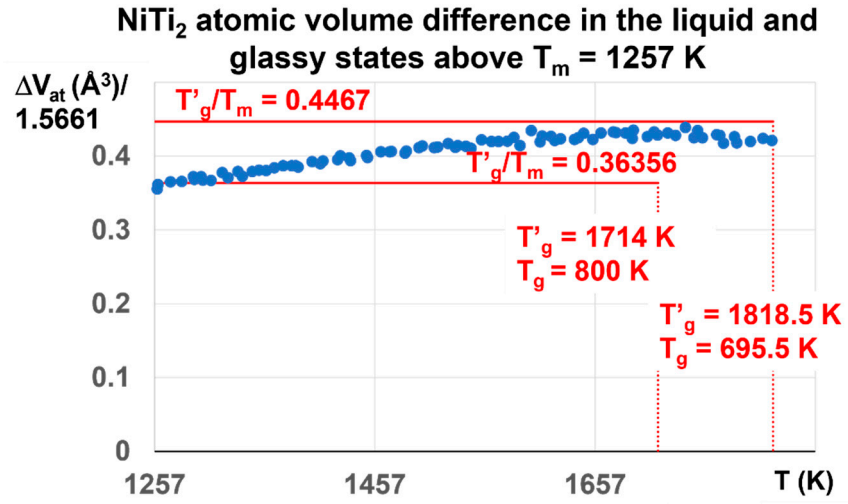


Figure 11. $NiTi_2$ atomic volume difference between liquid and glass above T_m = 1257 K. The initial liquid glass state at room temperature is characterized by T'_g = 1818.5 K and T_g = 695.5 K. Its enthalpy coefficient is expected to be equal 0.4467. The maximum calculated value is 0.4387 ± 0.01 at 1714 K. It begins to decrease and attain 0.36356 at T = 1931 K and zero at 2120 K in Figure 3. The influence of the glass phase with T'_g = 1818.5 still exists up to 1931 K. The glass phase disappears without first-order transition at 2120 K due to the prolongation of the glass state.

The atomic volume change at the melting temperature T_m = 1257 K is equal to the volume variation (ΔV = 1.5661 Å^3) of the melt between T_m and 2 T_m [34]. A new liquid glass state is stabilized at 300 K. The glass transition temperature T_g becomes equal to 695.5 K instead of 800 K after a cooling rate at 10^{12}−10^{13} K/s. The Phase 3 enthalpy coefficient $\Delta\varepsilon_{lg} = \varepsilon_{ls} - \varepsilon_{gs}$ is equal to 0.22335 at low temperatures, and corresponds to a volume change of 0.22335 × 1.5661 = 0.35, in agreement with that of Figure 8.

The ratio T'_g/T_m in Figure 11 is expected to be equal to 1.4467 for T'_g = 1818.5 K and T_g = 695.5 K and 1.36356 for T'_g = 1714 K and T_g = 800 K. Its maximum value is 1.4387 at T'_g = 1714 K instead of 1.4467. Above T_m = 1257 K, the dominant liquid glass phase with T'_g = 1818.5 K is progressively replaced by the liquid glass with T'_g = 1714 K and T_g = 800 K, because ΔV_{at} begins to decrease above 1714 K.

These results show that $\Delta\varepsilon$ progressively varies between the two maximum values $\theta_{n+} = \Delta\varepsilon$ = 0.4467 and 0.36356. The first-order transitions expected at 1714 K and 1818.5 K are not observed because the crystal melting in $NiTi_2$ extends up to 2120 K in Figure 3 at 10^{13} K/s. The glass fraction first increases with temperature from $\Delta\varepsilon$ = 0.22335 to 0.4387, and attains 0.36356 at 1931 K.

There is a competition between two glass phases. The first one has a glass transition temperature equal to T_{n+} = 2120 K, which is equal to the temperature T_{n+} of $NiTi_2$ full melting, as shown in Figure 12, studying the crystal melting temperature dependence with high heating rates at 10^{12}−10^{13} K/s. The transition is sharp with 10^{12} K/s, and continuous with 10^{13} K/s.

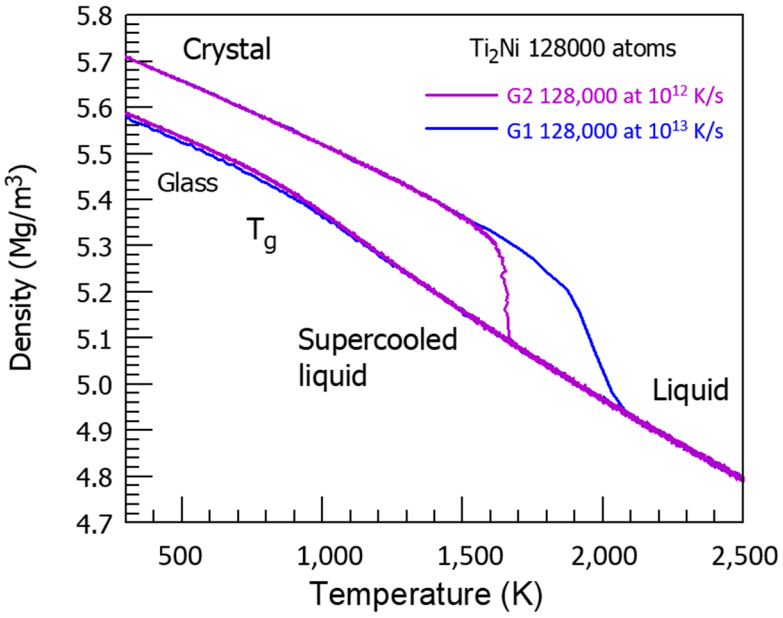


Figure 12. The $NiTi_2$ crystal density as a function of temperature at high heating rates. As indicated at 10^{13} K/s, the crystal is completely melted at 2120 K instead of T_0 = 1257 K at a low heating rate. The glass transition T'_g of a glass fraction equal to 0.68632 occurs at θ_{n+} = 0.68632 and T_{n+} = 1.68632 × T_0 = 2120 K with 0.68632 = 0.14085 + 0.18178 + 0.36369. The crystal melting starts at T_{n+} = 1891 K and θ_{n+} = 0.50454 = 0.14085 + 0.36369. At 10^{12} K/s, melting occurs at 1650 K, corresponding to θ_{n+} = (1650 − 1257)/1257 = 0.31265. The sum of singular coefficients (0.14085 + 0.18178) leads to (0.32263) and to θ_{n+} = 1663 K.

This temperature T_{n+}, being the liquid glass transition temperature, corresponds to θ_{n+} = 0.68632 equal to the sum of singular values (0.14085 + 0.18178 + 0.36369) of the enthalpy coefficient of Phase 3. The $NiTi_2$ melting starts earlier at T_{n+} = 1891 K and θ_{n+} = 0.50454 = 0.14085 + 0.36369, and is prolongated toward θ_{n+} = 0.68632. The second glass phase results from a first-order transition obeying to the nucleation law in Equation (7) with a weaker and weaker fraction $\Delta\varepsilon$. The maximum difference $\Delta\varepsilon$ increases up to 0.4387 without attaining T'_g/T_m = 0.4467, and declines toward zero at 2120 K. The first-order transition cannot take place at T'_g = 1714 K because the glass phase is prolongated by that of a liquid glass fraction equal to 0.686 with $T'_g = T_{n+}$ = 2120 K.

The two liquid states found by numerical simulations are already observed in Co–B melts [39]. The temperature-dependent liquid structures are studied in situ, measuring the magnetization. A magnetization anomaly in terms of the non-Curie–Weiss temperature dependence of magnetization was observed in the overheated state, demonstrating a temperature-induced liquid–liquid structure transition. This anomalous behavior was found to be a universal formula for the Co–B binary alloy system. The transition point at T_{n+} (called T_0 in the publication), above which there is a unique liquid state and below which two paramagnetic Curie temperatures (θ_p (L_I), θ_p (L_{II})) corresponding to two distinct kinds of liquids (i.e., high-magnetization liquid $(HML)_I$ and low-magnetization liquid $(LML)_{II}$), are measured. With the increased concentration of Co, T_{n+}, θ_p (L_I) and θ_p (L_{II}) shift to higher temperatures, and the Curie constants for the HML and LML decrease. Based on the location of T_{n+}, a guideline is drawn above the liquidus in the Co–B phase diagram.

As a conclusion of this chapter, the liquid glass states extend far above T_m. Table 2, after ref. [26], illustrates the positioning of liquid glasses in terms of connectivity and ordering increase (e.g., on temperature decrease).

Table 2. Phases of materials as function of connectivity and ordering of atomic constituents.

Degree of Connectivity. ***Degree of Ordering***	**Low**	**High**
High	Liquid crystals; Liquid quasi-crystals	Crystals; Quasi-crystals
Medium	Liquid glasses	Glass crystalline materials; Glass quasi-crystalline materials
Low	Melts	Glass [1]

[1] The connectivity between atomic species can be diminished not only by an increase of temperature: the irradiation of glasses, which breaks the interatomic chemical bonds, leads to fluidization of glasses [89].

The right column of Table 2 is for solid-like matter, which occurs when the degree of connectivity between atomic or molecular constituents is high. Here, we have glasses with a topologically disordered distribution of atoms or molecular species, or crystals. At a medium degree of order, we have composite materials composed of both vitreous, crystalline with periodicity, and even quasi-crystalline (QC) phases with nonperiodic order [29,90]. When the degree of connectivity is low, as shown in the second column of Table 2, we have fluid-like behavior of matter. It starts with melts containing icosahedral superclusters when there is low connectivity between species at a low degree of their ordering. If the degree of ordering becomes high, we have the case of liquid crystals, which is a distinct phase of matter observed between the crystalline (solid) and isotropic (liquid) states. The liquid glass state of matter was missing within classification of matter until recently, because it is a combination of both glassy and liquid fractions, which cannot be readily revealed, e.g., via X-ray diffraction. It is a flowing state of matter placed within a classification scheme at a low degree of connectivity characteristic to liquids, and has a medium degree of ordering because the fraction of glass within liquid adds some degree of ordering, being distinct from the molten state of matter at least by its symmetry signature, i.e., the Hausdorff dimensionality of bonds, which is D = 3 for glasses and D = 2.5 for liquids; see, e.g., Table 2 of Refs. [25,36,91–93].

5. Conclusions

The formation of liquid glasses induced by first-order transitions at temperatures $T_x < T_m$, with glass transition temperatures at $T_{n+} > T_m$ has been proposed many times during the last years. Glass transitions have been recently observed above T_m in the composite (ZIF-62) (Al-rich) (50/50), in tin, and in suspensions of ellipsoidal colloids. The existence of such liquid glasses can be extended by molecular dynamics simulations. $NiTi_2$ is chosen because its glass transition, at T_g = 800 K (T_m = 1257 K) and at high cooling rate, was initially determined by MD simulations, revealing structural changes at this glass transition via radial distribution functions. Applying very high pressures attaining 1000 GPa at 1000 K, and abruptly decreasing the temperature from the liquid state to 300 K or increasing the temperature from 300 K to 1000 K from the glass state, induces a weak reversible first-order transition of the atomic volume with ΔV_{at} = 0.0098 Angström^3. A new liquid glass state exists at 300 K up to 2120 K after reduction of the pressure to one bar, characterized by an atomic volume difference at 300 K, with the classical glass with T_g = 800 K being 35.69 times higher than under a pressure of 1000 GPa. This decrease of ΔV_{at} with pressure is associated with the strong increase of T_m. $[T_m\ (1000\ GPa)/T_0]^2$ is equal to 35.69 because the entropy of melting linearly increases with pressure instead of being constant. The melting temperature T_m of $NiTi_2$ would attain 6779 K for T_0 = 1257 K. We control this relation, calculating the melting temperatures of copper and iron as a function of pressure using known experimental values at various low pressures. Our extrapolated values agree with other extrapolations for copper and iron. The observed first-order transitions show that this liquid glass exists up to temperatures $T_{n+} = 1.686\ T_m$, and that memory effects are present at ambient pressure by abruptly varying the temperature under extreme high pressures. Liquid glasses are a new class of materials which

deeply disrupt the concept of homogenous liquids without memory of their solid and glass transformations below T_m.

The continuous increase of the volume difference ΔV_{at} between the liquid and the glass from 300 K up to T'_g = 1714 K shows that the volume fraction involved in this glass fraction attains ~44%.

This finding could lead to a reconsideration of glass formation in volcanic rocks. Up to now, the explanation is based on the high content of SiO_2 in amorphous rocks with $T_g \leq 1473$ K. A first-order transition at $T'_g = 2\,T_m - T_g \leq 2519$ K could exist during cooling or, in the absence of spontaneous first-order transition at $T'_g \leq 2519$ K, and depending on the thermal history, a first-order transition could be induced during the simultaneous pressure and temperature decreases at different rates.

Author Contributions: Conceptualization, R.F.T. and M.I.O.; methodology, R.F.T.; software, R.F.T.; validation, R.F.T. and M.I.O.; formal analysis, R.F.T.; investigation, R.F.T. and M.I.O.; data curation, R.F.T.; writing—original draft preparation, R.F.T.; writing—review and editing, R.F.T. and M.I.O. All authors have read and agreed to the published version of the manuscript.

Funding: This research received no external funding.

Institutional Review Board Statement: Not applicable.

Informed Consent Statement: Not applicable.

Data Availability Statement: Data supporting reported results can be found within references provided.

Acknowledgments: MD simulation results for $NiTi_2$ were provided by Dmitri V. Louzguine-Luzgin.

Conflicts of Interest: The authors declare no conflict of interest.

References

1. Turnbull, D. Kinetics of solidification of supercooled liquid mercury. *J. Chem. Phys.* **1952**, *20*, 411. [CrossRef]
2. Turnbull, D.; Fisher, J.C. Rate of nucleation in condensed systems. *J. Chem. Phys.* **1949**, *17*, 71–73. [CrossRef]
3. Kelton, K.F. Crystal nucleation in liquids and glasses. *Sol. State Phys.* **1991**, *45*, 75–177.
4. Vinet, P.; Magnusson, L.; Frederikssen, H.; Desré, P.J. Correlations between surface and interface energies with respect to crystal nucleation. *J. Colloid Interf. Sci.* **2002**, *255*, 363–374. [CrossRef]
5. Tournier, R.F. Crystallization of supercooled liquid elements induced by superclusters containing magic atom numbers. *Metals* **2014**, *4*, 359–387. [CrossRef]
6. Yang, B.; Perepezko, J.H.; Schmelzer, J.W.P.; Gao, Y.; Schick, C. Dependence of crystal nucleation on prior liquid overheating by differential fast scanning calorimeter. *J. Chem. Phys.* **2014**, *140*, 104513. [CrossRef]
7. Tournier, R.F. Presence of intrinsic growth nuclei in overheated and undercooled liquid elements. *Phys. B Condens. Matter* **2007**, *392*, 79–91. [CrossRef]
8. Tournier, R.F. Thermodynamic origin of the vitreous transition. *Materials* **2011**, *4*, 869–892. [CrossRef] [PubMed]
9. Tournier, R.F. Thermodynamic and kinetic origin of the vitreous transition. *Intermetallics* **2012**, *30*, 104–110. [CrossRef]
10. Tournier, R.F. Lindemann's rule applied to the melting of crystals and ultra-stable glasses. *Chem. Phys. Lett.* **2016**, *651*, 198–202, Erratum in *Chem. Phys. Lett.* **2017**, *675*, 174. [CrossRef]
11. Tournier, R.F. Glass phase and other multiple liquid-to-liquid transitions resulting from two-liquid competition. *Chem. Phys. Lett.* **2016**, *665*, 64–70. [CrossRef]
12. Wool, R.P. Twinkling fractal theory of the glass transition. *J. Polym. Sci. Part B Polym. Phys.* **2008**, *46*, 2765–2778. [CrossRef]
13. Wool, R.P.; Campanella, A. Twinkling fractal theory of the glass transition: Rate dependence and time-temperature superposition. *J. Polym. Sci. Part B Polym. Phys.* **2009**, *47*, 2578–2589. [CrossRef]
14. Stanzione, J.F., III; Strawhecker, K.E.; Wool, R.P. Observing the twinkling nature of the glass transition. *J. Non-Cryst. Sol.* **2011**, *357*, 311. [CrossRef]
15. Tournier, R.F. First-order transitions in glasses and melts induced by solid superclusters nucleated by homogeneous nucleation instead of surface melting. *Chem. Phys.* **2019**, *524*, 40–54. [CrossRef]
16. Hornboll, L.; Yue, Y. Enthalpy relaxation in hyperquenched glasses of different fragility. *J. Non-Cryst. Sol.* **2008**, *354*, 1832–1870. [CrossRef]
17. Hu, C.; Zhang, C.; Yue, Y. Thermodynamic anomaly of the sub-Tg relaxation in hyperquenched metallic glasses. *J. Chem. Phys.* **2013**, *138*, 174508. [CrossRef]
18. Jian, Q.K.; Wang, X.D.; Nie, X.P.; Zhang, G.Q.; Ma, H.; Fecht, H.J.; Bendnarck, J.; Franz, H.; Liu, Y.G.; Cao, Q.P.; et al. Zr-(Cu,Ag)-Al bulk metallic glasses. *Acta Mater.* **2008**, *56*, 1785–1796. [CrossRef]

19. Inoue, A.; Zhang T: Masumoto, T. The structural relaxation and glass transition of La-Al-Ni and Zr-Al-Cu amorphous alloys with a significant supercooled liquid region. *J. Non-Cryst. Sol.* **1992**, *150*, 396. [CrossRef]
20. Zhou, S.H.; Schmid, J.; Sommer, F. Thermodynamic properties of liquid, undercooled liquid and amorphous Al-Cu-Zr and Al-Cu-Ni-Zr. *Thermochim. Acta* **1999**, *339*, 79–91. [CrossRef]
21. Wang, L.-M.; Borick, S.; Angell, C.A. An electrospray technique for hyperquenched glass calorimetry studies: Propylene glycol and di-n-butylphthalate. *J. Non-Cryst. Sol.* **2007**, *353*, 3829–3837. [CrossRef]
22. Jabrane, S.; Létoffé, J.M.; Claudy, P. Vitrification and crystallization in the R(−)1,2-propanediol-S(+)1,2-propadeniol system. *Thermchim. Acta* **1995**, *258*, 33–47. [CrossRef]
23. Ojovan, M.I.; Travis, K.P.; Hand, R.J. Thermodynamic parameters of bonds in in glassy materials from viscosity temperature relationships. *J. Phys. Cond. Matter.* **2007**, *19*, 415107. [CrossRef] [PubMed]
24. Ojovan, M.I.; Lee, W.E. Connectivity and glass transition in disordered oxide systems. *J. Non-Cryst. Sol.* **2010**, *356*, 2534–2540. [CrossRef]
25. Ojovan, M.I. Ordering and structural changes at the glass-liquid transition. *J. Non-Cryst. Sol.* **2013**, *382*, 79. [CrossRef]
26. Ojovan, M.I. The modified random network model within the configuron percolation theory. *Ceramics* **2021**, *4*, 121–134. [CrossRef]
27. Tournier, R.F. Amorphous ices. In *Encyclopedia of Glass Science, Technology, History, and Culture*; Richet, P., Conradt, R., Takada, A., Dyon, J., Eds.; Wiley & Sons: Hoboken, NJ, USA, 2021.
28. Tournier, R.F. Homogeneous nucleation of phase transformations in supercooled water. *Phys. B* **2020**, *579*, 411895. [CrossRef]
29. Tournier, R.F.; Ojovan, M.I. Undercooled phase behind the glass phase with superheated medium-eange order above glass transition temperature. *Phys. B* **2021**, *602*, 412542. [CrossRef]
30. Scher, H.; Zallen, R. Critical density in percolation processes. *J. Chem. Phys.* **1970**, *53*, 3759–3761. [CrossRef]
31. Tournier, R.F. Liquid-liquid transitions due to melting temperatures of residual glassy phases expected in $Pt_{57}Cu_{23}P_{20}$. *Aspects Min. Sci.* **2022**, *8*, 979–989. [CrossRef]
32. Tournier, R.F.; Ojovan, M.I. Multiple melting temperatures in glass-forming melts. *Sustainability* **2022**, *14*, 2351. [CrossRef]
33. Tournier, R.F.; Ojovan, M.I. Building and breaking bonds by homogenous nucleation in glass-forming melts leading to three liquid states. *Materials* **2021**, *14*, 2287. [CrossRef] [PubMed]
34. Tournier, R.F. Multiple glass transitions in bismuth and tin beyond melting temperatures. *Metals* **2022**, *12*, 2085. [CrossRef]
35. Scaliet, C.; Berthier, L. Rejuvenation and memory effects in a structural glass. *Phys. Rev. Lett.* **2019**, *122*, 255502. [CrossRef]
36. Ojovan, M.I.; Louzguine Luzgin, D.V. Revealing Structural Changes at Glass Transition via Radial Distribution Functions. *J. Phys. Chem.* **2020**, *124*, 3186–3194. [CrossRef]
37. Tournier, R.F.; Ojovan, M.I. Dewetting Temperatures of Prefrozen and Grafted Layers in Ultrathin Films Viewed as Melt-Memory Effects. *Phys. B* **2021**, *611*, 412796. [CrossRef]
38. Na, J.H.; Corona, S.L.; Hoff, A.; Johnson, W.L. Observation of an apparent first-order glass transition in ultrafragile Pt-Cu-P bulk metallic glasses. *Proc. Natl. Acad. Sci. USA* **2020**, *117*, 2779–2787. [CrossRef]
39. He, Y.-X.; Li, J.; Wang, J.; Kou, H.; Beaugnon, E. Liquid-liquid structure transition and nucleation in undercooled Co-B eutectic alloys. *Appl. Phys. A* **2017**, *123*, 391. [CrossRef]
40. Yu, Y.; Lv, L.; Wang, X.-Y.; Zhu, B.; Huang, Z.-Y.; Zu, F.-Q. Influence of melt overheating treatment on solidification behavior of BiTe-based alloys at different cooling rates. *Mater. Des.* **2015**, *88*, 743–750. [CrossRef]
41. Xu, W.; Sandor, M.T.; Yu, Y.; Ke, H.-B.; Zhang, H.P.; Li, M.-Z.; Wang, W.-H.; Liu, L.; Wu, Y. Evidence of liquid-liquid transition in glass-forming $La_{50}Al_{35}Ni_{15}$ melt above liquidus temperature. *Nat. Commun.* **2015**, *6*, 7696. [CrossRef]
42. Tournier, R.F.; Beaugnon, E. Texturing by cooling a metallic melt in a magnetic field. *Sci. Technol. Adv. Mater.* **2009**, *10*, 014501. [CrossRef] [PubMed]
43. Legrand, B.A.; Chataigner, D.; Perrier de la Bathie, R.; Tournier, R.F. Orientation by solidification in a magnetic field. A new process to texture SmCo compounds used as perrmanent magnets. *J. Magn. Magn. Mater.* **1997**, *173*, 20. [CrossRef]
44. Kim, Y.H.; Kiraga, K.; Inoue, A.; Masumoto, T.; Jo, H.H. Crystallization and high mechanical strengthof Al-based amorphous alloys. *Mater. Trans.* **1994**, *35*, 293–302. [CrossRef]
45. Popel, P.S.; Sidorov, V.E. Microheterogeneity of liquid metallic solutions and its influence on the structure and propertes of rapidly quenched alloys. *Mater. Sci. Eng.* **1997**, *226–228*, 237–244. [CrossRef]
46. Yue, Y. Experimental evidence for the existence of an ordered structure in a silicate liquid above its liquidus temperature. *J. Non-Cryst. Sol.* **2004**, *345–346*, 523–527. [CrossRef]
47. Wang, L.; Bian, X.; Liu, J. Discontinuous structural phase transition of liquid metal and alloys. *Phys. Lett. A* **2004**, *326*, 429–435. [CrossRef]
48. Way, C.; Wadhwa, P.; Busch, R. The influence of shear rate and temperature on the viscosity and fragility of the $Zr_{41.2}Ti_{13.8}Cu_{12.5}Ni_{10.0}Be_{22.5}$ metallic-glass-forming liquid. *Acta Mater.* **2007**, *55*, 2977–2983. [CrossRef]
49. Bian, X.F.; Sun, B.A.; Hu, L.N.; Jia, Y.B. Fragility of superheated melts and glass-forming ability in Al-based alloys. *Phys. Lett. A* **2005**, *335*, 61–67. [CrossRef]
50. Wei, S.; Yang, F.; Bednarcik, J.; Kaban, I.; Shuleshova, O.; Meyer, A.; Busch, R. Liquid-liquid transition in a strong bulk metallic glass-forming liquid. *Nat. Commun.* **2013**, *4*, 2083. [CrossRef]
51. Lan, S.; Ren, Y.; Wei, X.Y.; Wang, B.; Gilbert, E.P.; Shibayama, T.; Watanabe, S.; Ohnuma, M.; Wang, X.-L. Hidden amorphous phase and reentrant supercooled liquid in Pd-Ni-P metallic glass. *Nat. Commun.* **2017**, *8*, 14679. [CrossRef]

52. Hu, Q.; Sheng, H.C.; Fu, M.W.; Zeng, X.R. Influence of melt temperature on the Invar effect in $(Fe_{71.2}B_{24}Y_{4.8})_{96}Nb_4$ bulk metallic glasses. *J. Mater. Sci.* **2019**, *48*, 6900–6906.
53. Jiang, H.-R.; Bochtler, B.; Riegler, X.-S.; Wei, S.S.; Neuber, N.; Frey, M.; Gallino, I.; Busch, R.; Shen, J. Thermodynamic and kinetic studies of the Cu-Zr-Al(-Sn) bulk metallic glasses. *J. Alloys Comp.* **2020**, *844*, 156126. [CrossRef]
54. Chen, E.-Y.; Peng, S.-X.; Peng Michiel, M.D.; Vaughan, G.B.M.; Yu, Y.; Yu, H.-B.; Ruta, B.; Wei, S.; Liu, L. Glass-forming ability correlated with the liquid-liquid transition in $Pd_{42.5}Ni_{42.5}P_{15}$ alloy. *Scr. Mater.* **2021**, *193*, 117–121. [CrossRef]
55. Tournier, R.F.; Ojovan, M.I. Comments about a recent publication entitled entitled "Improving glass forming ability of off-eutectic metallic glass formers by manipulating primary crystallization reactions". *Scr. Mater.* **2021**, *205*, 114039. [CrossRef]
56. Zeng, Y.Q.; Yu, J.S.; Tian, Y.; Hirata, A.; Fujita, T.; Zhang, X.H.; Nishiyama, N.; Kato, H.; Jiang, J.Q.; Inoue, A.; et al. Response to the commentary by Robert Tournier and Michael Ojovan on our publication entitled "Improving glass forming ability of off-eutectic metallic glass formers by manipulating primary crystallization reactions". *Scr. Mater.* **2021**, *205*, 114035. [CrossRef]
57. Tariq, M.; Dolynchuk, O.; Thurn-Albrecht, T. Effect of substrate interaction on thermodynamics of prefreezing. *Macromolecules* **2019**, *52*, 9140–9148. [CrossRef]
58. Galymzianov, B.N.; Doronina, M.A.; Mokshin, A.V. Arrhenius cross-over temperature of glass-forming liquids predicted by an articial network. *Materials* **2023**, *16*, 1127. [CrossRef]
59. An, Q.; Johnson, W.L.; Samwer, K.; Corona, S.L.; Goddart, W.A., III. Formation of two glass phases in binary Cu-Ag liquid. *Acta Mater.* **2020**, *195*, 274–281.
60. Becker, S.; Devijver, E.; Molinier, R.; Jakse, N. Glass-forming ability of elemental zirconium. *Phys. Rev. B* **2020**, *102*, 104205. [CrossRef]
61. An, Q.; Johnson, W.L.; Samwer, K.; Corona, S.L.; Goddard, W.A., III. First-order transition in liquid Ag to the heterogeneous G-Phase. *J. Phys. Chem. Lett.* **2020**, *11*, 632–645. [CrossRef] [PubMed]
62. Tournier, R.F.; Ojovan, M.I. Prediction of second melting temperatures already observed in pure elements by molecular dynamics simulations. *Materials* **2021**, *14*, 6509. [CrossRef] [PubMed]
63. Popel, P.S.; Chikova, O.A.; Matveev, V.M. Metastable colloidal states of liquid metallic solutions. *High Temp. Mater. Proc.* **1995**, *4*, 219–233. [CrossRef]
64. Louzguine-Luzgin, D.V.; Belosludov, R.; Saito, M.; Kawazoe, Y.; Inoue, A. Glass transition of Ni: Calculation, Prediction, and experiment. *J. Appl. Phys.* **2008**, *104*, 123529. [CrossRef]
65. Zhou, C.; Hu, L.; Sun, Q.; Qin, J.; Brian, X.; Yue, Y. Indication of liquid-liquid phase transition in CuZr-based melts. *Appl. Phys. Lett.* **2013**, *103*, 171904. [CrossRef]
66. Bennett, T.D.; Yue, Y.; Li, P.; Qiao, A.; Tao, H.; Greaves, N.G.; Richards, T.; Lampronti, G.I.; Redfern, S.A.T.; Blanc, F.; et al. Melt-quenched glasses of metal-organic frameworks. *J. Am. Chem. Soc.* **2016**, *138*, 3484–3492. [CrossRef]
67. Longley, L.; Calahoo, C.; Limbach, R.; Xia, Y.; Tuffnell, J.M.; Sapnik, A.F.; Thorne, M.F.; Keeble, D.S.; Keen, D.A.; Wondraczek, L.; et al. Metal-organic framework and inorganic glass composites. *Nat. Commun.* **2020**, *11*, 5800. [CrossRef] [PubMed]
68. Xu, L.; Wang, Z.; Chen, J.; Chen, S.; Yang, W.; Ren, Y.; Zuo, X.; Zeng, J.; Wu, Q.; Sheng, H. Folded network and structural transition in molten tin. *Nat. Commun.* **2022**, *13*, 126. [CrossRef]
69. Roller, J.; Laganopan, A.; Meijer, J.-M.; Fuchs, M.; Zumbusch, A. Observation of liquid glass in suspension of ellipsoidal colloids. *Proc. Natl. Acad. Sci. USA* **2021**, *118*, e2018072118. [CrossRef] [PubMed]
70. Takaiwa, D.; Atano, I.; Koga, K.; Tanaka, H. Phase diagram of water in carbon nanotubes. *Proc. Natl. Acad. Sci. USA* **2008**, *105*, 39–43. [CrossRef]
71. Tournier, R.F.; Bossy, J. ^{4}He glass phase: A model for liquid elements. *Chem. Phys. Lett.* **2016**, *658*, 282–286. [CrossRef]
72. Tournier, R.F. Validation of non-classical homogeneous nucleation model for G-glass and L-glass formations in liquid elements with recent molecular dynamics simulations. *Scr. Mater.* **2021**, *199*, 113859. [CrossRef]
73. Bazlov, A.I.; Louzguine-Luzguin, D.V. Crystallization of FCC and BCC liquid metals studied by molecular dynamics simulation. *Metals* **2020**, *10*, 1532.
74. Buchwitz, M.; Adlwarth-Dieball, R.; Ryder, P.L. Kinetics of crystallization of amorphous Ti_2Ni. *Act. Met. Mater.* **1993**, *41*, 1885–1892. [CrossRef]
75. Plimpton, S.J. Fast prallel algorithms for short-range molecular dynamics. *J. Comp. Phys.* **1995**, *117*, 1. [CrossRef]
76. Wang, Z.; Chen, C.L.; Ketov, S.V.; Akagi, K.; Tsarkov, A.A.; Ikuara, Y.; Louzguine-Luzgin, D.V. Local chemical ordering within the incubation period as a trigger for nanocrystallization of a highly supercooled Ti-based liquid. *Mater. Design.* **2018**, *156*, 504–513. [CrossRef]
77. Nose, S. A unified formulation of the constant temperature molecular dynamics methods. *J. Chem. Phys.* **1984**, *81*, 511. [CrossRef]
78. Hoover, W.J. Canonical dynamics, Equilibrium phase-space distributions. *Phys. Rev. A* **1985**, *31*, 1965. [CrossRef]
79. Beredsen, H.J.C.; Postma, J.P.M.; Van Gunsteren, W.F.; DiNola, A.; Haak, J.R. Molecular dynamics with stable coupling to an external bath. *J. Chem. Phys.* **1984**, *81*, 3684–3690. [CrossRef]
80. Otsuka, K.; Ren, X. Martensitic transformations in nonferrous shape memory alloys. *Mater. Sci. Eng.* **1999**, *273–275*, 89–105. [CrossRef]
81. Ezenwa, I.C.; Yoshino, T. Electrical Resistivity of Cu and Au at High Pressure above 5 GPa: Implications for the Constant Electrical Resistivity Theory along the Melting Curve of the Simple Metals. *Materials* **2021**, *14*, 5476. [CrossRef]
82. Ho, K.H.; Nguyen, N.H. High pressure melting curves of silver, gold and coppe. *AIP Adv. Pub.* **2013**, *3*, 112125.

83. Cohen, L.H.; Klement, W., Jr.; Kennedy, G.C. Melting of copper, silver and gold at high pressures. *Phys. Rev.* **1966**, *145*, 519. [CrossRef]
84. Pham, D.T.; Nguyen, Q.H.; Bui, D.T.; Pham, D.T. Melting curve of metals Cu, Ag and Au under pressure. *Mod. Phys. Lett. B* **2016**, *30*, 1550273.
85. Goyal, M. Melting temperature of metal under pressure. *Chin. J. Phys.* **2020**, *66*, 453–460. [CrossRef]
86. Japel, S.; Schwager, B.; Boehler, R.; Ross, M. Melting of copper and nickel at high pressure. *Phys. Rev. Lett.* **2005**, *95*, 167801. [CrossRef]
87. Aquilanti, G.; Rapananti, A.T.; Karandikar, A.; Boehler, R. Melting of iron determined by X-ray absorption spectroscopy to 100 GPa. *Proc. Natl. Acad. Sci. USA* **2015**, *112*, 12042–12045. [CrossRef] [PubMed]
88. Sinmyo, R.; Hirose, K.; Ohishi, Y. Melting curve of iron to 290 GPa determined in a resistance-heated diamond-anvil cell. *Earth Planet. Sci. Lett.* **2019**, *510*, 45–52. [CrossRef]
89. Ojovan, M.I. The Flow of Glasses and Glass–Liquid Transition under Electron Irradiation. *Int. J. Mol. Sci.* **2023**, *24*, 12120. [CrossRef] [PubMed]
90. Kurtuldu, G.; Shamlaye, K.F.; Löffler, J. Metastable quasi-crystal induced nucleation in a bulk glass-forming melt. *Proc. Natl. Acad. Sci. USA* **2018**, *115*, 6123–6128. [CrossRef]
91. Ojovan, M.I. Glass formation. In *Encyclopedia of Glass Science, Technology, History, and Culture*; Richet, P., Conradt, R., Takada, A., Dyon, J., Eds.; Wiley: Hoboken, NJ, USA, 2021; 1568p, pp. 249–259. [CrossRef]
92. Ojovan, M.I.; Tournier, R.F. On structural rearrangements near the glass transition temperature in amorphous silica. *Materials* **2021**, *14*, 5235. [CrossRef] [PubMed]
93. Ojovan, M.I.; Louzguine-Luzgin, D.V. On Structural Rearrangements during the Vitrification of Molten Copper. *Materials* **2022**, *15*, 1313. [CrossRef] [PubMed]

Disclaimer/Publisher's Note: The statements, opinions and data contained in all publications are solely those of the individual author(s) and contributor(s) and not of MDPI and/or the editor(s). MDPI and/or the editor(s) disclaim responsibility for any injury to people or property resulting from any ideas, methods, instructions or products referred to in the content.